



## OPEN ACCESS

## EDITED BY

Yifei Zhao,  
Nanjing Normal University, China

## REVIEWED BY

Wenfang Zhang,  
Nanjing Institute of Geography and  
Limnology (CAS), China  
Liang Zhou,  
Jiangsu Normal University, China

## \*CORRESPONDENCE

Chao Zhan  
zhanchaodd@126.com  
Xianbin Liu  
liuxb\_801@163.com

†These authors have contributed  
equally to this work

## SPECIALTY SECTION

This article was submitted to  
Coastal Ocean Processes,  
a section of the journal  
Frontiers in Marine Science

RECEIVED 19 October 2022

ACCEPTED 18 November 2022

PUBLISHED 09 December 2022

## CITATION

Wang Q, Zeng L, Zhan C, Liu X,  
Wang L, Cheng S and Cui B (2022)  
Geomorphologic evolution of the  
shallow-buried abandoned Yellow  
River delta during the last 2000 years.  
*Front. Mar. Sci.* 9:1073961.  
doi: 10.3389/fmars.2022.1073961

## COPYRIGHT

© 2022 Wang, Zeng, Zhan, Liu, Wang,  
Cheng and Cui. This is an open-access  
article distributed under the terms of  
the [Creative Commons Attribution  
License \(CC BY\)](https://creativecommons.org/licenses/by/4.0/). The use, distribution  
or reproduction in other forums is  
permitted, provided the original  
author(s) and the copyright owner(s)  
are credited and that the original  
publication in this journal is cited, in  
accordance with accepted academic  
practice. No use, distribution or  
reproduction is permitted which does  
not comply with these terms.

# Geomorphologic evolution of the shallow-buried abandoned Yellow River delta during the last 2000 years

Qing Wang<sup>†</sup>, Lin Zeng<sup>†</sup>, Chao Zhan<sup>\*</sup>, Xianbin Liu<sup>\*</sup>,  
Longsheng Wang, Shanshan Cheng and Buli Cui

Institute of Coastal Research, Ludong University, Yantai, China

Different from the continuous development of many river deltas since the major Holocene transgression, the modern Yellow River delta (YRD) remained for nearly 1000 years (from 893 AD to 1855 AD) in an abandonment state, until after 1855 AD when it was buried after the Yellow River entered the sea *via* Lijin. In this study we used optically stimulated luminescence (OSL) dating and grain size and sedimentary facies analysis of four borehole cores, combined with an analysis of landform morphology, to reconstruct the history of the ancient abandoned YRD. The results indicate that after the delta was abandoned due to the reduced sediment supply by the Yellow River in 893 AD, a sandy coast developed under the influence of wave erosion, and offshore shell ridges were formed beyond the coastline. During the interval from the Medieval Warm Period (MWP) to the Little Ice Age (LIA), driven by climate change and storm surges, the shell ridges migrated laterally, widened and rose, while sediment accumulation in the landward-side interfluvial floodplains was relatively weak. This configuration subsequently constituted a coastal highland – plain depression system. After 1077 AD, this system, together with the abandoned delta, was eroded by the Daqing River estuary. After 1855 AD, the abandoned delta landform system was completely buried by Yellow River sediments, and the wave-controlled sandy coast was transformed to a tide-controlled silt-mud coast. We summarize these findings in the form of a geomorphic model of the evolution of the abandoned delta from the MWP to the LIA. Overall, our results highlight the geomorphic effects of the sediment-laden river delta and the response of the abandoned delta geomorphic system on the millennial timescale, and they provide a theoretical foundation for predicting the geomorphic evolution of a major river delta on different timescales, against the background of global change.

## KEYWORDS

coastal geomorphology, storm surges, luminescence dating, reduced sediment supply, abandoned delta

## Introduction

The geomorphologic evolution of deltas on different timescales is strongly influenced by the interactions of various components of the Earth system, including fluvial sediment supply and climate change. Coastal erosion has affected several major river deltas in the 20<sup>th</sup> century due to the reduction of fluvial sediment supply (Zhou et al., 2014; Chamberlain et al., 2018; Dai et al., 2018), including changes in erosion and deposition in submerged deltas (Dai et al., 2014; Jiang et al., 2017; Xu et al., 2020) and tidal flat coarsening (Zeng et al., 2021). Several studies have shown that the reduction of fluvial sediment supply can lead to delta abandonment and the transformation of deltas from a constructive to a destructive phase, in the course of the so-called 'delta cycle' (Roberts, 1997; Stanley and Warne, 1998; Nienhuis et al., 2013). Although fluvial sediment supply to the sea may not cease completely, river breaches (Jerolmack and Mohrig, 2007; Ganti et al., 2016), sediment redistribution (Giosan et al., 2005), dam interception, channelization, and other consequences of human activities (Phillips et al., 2004; Syvitski et al., 2009), can result in a decreased sediment supply and the consequent inability of delta plains to accommodate sediment accumulation through flooding, leaving many deltas in a state of 'quasi-wasting'. For example, the operation of the Aswan Dam has sharply reduced the sediment delivered from the Nile to the estuary, and sediment flux into the sea is almost nil, thus directly caused the coastal retreat of the entire Nile delta (Stanley and Warne, 1994). About 70% of the sediment load from upstream of the Yangtze River entrapped in the reservoir for the impacts of the world's largest dam, Three Gorges Dam (Dai et al., 2014, 2018). Suffering from a lack of sediments, the Yangtze delta is facing the threats of erosional retreat of the shoreline, and local government have to build a large number of levees to ensure delta sustainability. Meanwhile, the tidal forcing in the Yangtze delta has redistributed subaqueous sediment back into the delta plain, offsetting the negative effect of fluvial sediment reduction to some extent (Zhang et al., 2022). However, due to the temporal limitations of hydrological records, the time span of this type of research is typically from tens to hundreds of years, and few studies have focused on the effects of a reduced sediment supply on delta geomorphology on the millennial scale. The erosion of coastal deltas in China has occurred in the context of the construction of a large number of reservoirs, combined with soil and water conservation programs, since the 1950s, with a time span of only decades.

However, on the millennial timescale, the effects of a reduction of fluvial sediment supply on delta geomorphology may differ from those on the scale of decades to centuries. For example, the conversion from a silt-mud coast to a sandy coast may occur in several coastal contexts (Chen, 1980; 1982; Huang et al., 1989), and there may be changes in vertical accretion/pedogenesis intensity of delta interfluvial plains caused by changes in flooding. Historical documents show that the

Yellow River delta (YRD) maintained an overall abandonment state for nearly 1000 years, during 893 AD–1855 AD, due to the diversion of the lower reaches of the Yellow River (Tan, 1975; Guo, 1980; Zhuang et al., 1991). Therefore, a study of the geomorphic evolution of the abandoned YRD during this period may improve our understanding of the effects of a reduced fluvial sediment supply on the geomorphology of coastal deltas, on the millennial scale.

Climate change can affect the incidence and intensity of storms, wave action, sea ice and rainfall, with direct effects on estuarine and coastal sedimentary dynamics (Pryor and Barthelmie, 2010; Burvingt et al., 2018; Gopikrishna and Deo, 2018; Ning et al., 2018). For example, storms can have major effects on estuarine deltaic intertidal landforms, in terms of both erosion and deposition (Yang et al., 2019), and storms and wave action can lead to coastal erosion and the coarsening of beach deposits (Spencer et al., 2015; Bacino et al., 2019). Waves have become the principal driving force for shaping the topography of beaches during storms (Janssen-Stelder, 2000), leading to the landward movement of coastal dunes and significant erosion and deposition of underwater slopes (Li et al., 2019). The erosion of beaches and dunes during storms provides an important sediment source for lagoons and salt marshes (Brooks et al., 2017; Swindles et al., 2018). Besides erosion, storm surges can also affect sediment accumulation. For example, in the case of sandbar-lagoon systems, storm surges can cause severe erosion of sandbars (Sallenger, 2000; Houser et al., 2008; Eisemann et al., 2018; Li et al., 2019), and frequent storm surges can even lead to their disintegration, sinking and disappearance (FitzGerald et al., 2008). However, storm surge waves can also transport sediment eroded from sand bars, leading to sediment accumulation by other landforms, thus forming a new sand bar-lagoon system (Koiwa et al., 2018). Evidence from stalagmite  $\delta^{18}\text{O}$  and  $\delta^{13}\text{C}$  records shows the period between 892AD–1482AD was a time of warm climate known as the Medieval Warm Period (MPW), and the period between 1482AD–1894AD was a time of regional cooling known as the the Little Ice Age (LIA; Wang, 2015). The interval of 893 AD–1855 AD saw the formation, evolution and burial of the abandoned YRD. Thus, the abandonment of the ancient delta (893AD) approximately coincided with the beginning of the Medieval Warm Period, while its subsequent geomorphic evolution occurred during the Medieval Warm Period and the Little Ice Age, while its burial occurred prior to the end of the latter. The climatic fluctuations during this period probably affected the frequency and intensity of storm surges in the Bohai Sea with consequences for coastal sedimentary dynamics and geomorphic evolution. Therefore, the abandoned YRD can potentially provide a case study of the effects of climate change on the geomorphology of coastal deltas, and provide a theoretical basis and methodological support for predicting the evolution of deltaic landforms on a millennial timescale, against the background of global change.

In this study, we carried out a detailed sedimentological and grain-size study of four borehole cores from the YRD, which was combined with optically stimulated luminescence (OSL) dating, which enabled the high-resolution stratigraphic correlation of the cores. Our specific objectives were: (1) To reconstruct the topography and spatiotemporal distribution of the former coastline of the ancient abandoned Yellow River Delta during its abandonment stage, based on sedimentary facies correlation and an OSL chronology of the boreholes, combined with the published  $^{14}\text{C}$  ages of shell ridges. (2) To use the results to develop a model of the geomorphic evolution of the shallow-buried abandoned YRD during the interval spanning the Medieval Warm Period and the Little Ice Age. (3) Overall, to elucidate the response of an abandoned delta system to a reduction in sediment supply and climate change.

## Regional setting

The modern YRD, with Ninghai at its vertex, starts from the mouth of the Taoer River in the north and ends at the mouth of the Zhimai River in the south; the total land area is  $\sim 6000\text{ km}^2$  (Guo, 1980). Since 1855, the main channel of the Yellow River has generally flowed northeastward, forming a fan-shaped landform extending in that direction (Chen, 1982). The terrain is oriented southeast-northeast, and is high in the center and low on both sides, and high in the southwest and low in the northeast (Figure 1). Since avulsion have occurred frequently in the lower Yellow River, the Yellow River delta in the broad sense is thought to have been formed since approximately 6000 yr BP (Xue, 1993). The YRD has an intermittent development history compared to the continuous development of many deltas since the Holocene maximum transgression (Hoitink et al., 2017; Gao et al., 2019; Gugliotta and Saito, 2019). Before 40 BC the Jishui River estuary was located in this area, with a sandy coast on both sides (Tan, 1975) (Figure 1). According to historical documents, there have been two major stages of delta development and one delta abandonment stage during the past 2000 years (Gao et al., 1989). During 40 BC–893 AD, the Yellow River entered the Bohai Sea through Lijin, forming the ancient YRD; the abandoned delta state was subsequently maintained for nearly 1000 years, during 893 AD–1855 AD, from the Medieval Warm Period (MWP) to Little Ice Age (LIA) (Wang et al., 2015). In 1855 AD, after the Yellow River was diverted from northern Jiangsu to the Yellow Sea and then to Lijin, and the entire abandoned delta was rapidly buried, forming the modern YRD (Gao et al., 1989). Thus, frequent abandonment and discontinuous accumulation have characterized the geomorphic evolution of the YRD. Although its geomorphic history spans only  $\sim 2000$  years from the ancient YRD to the modern YRD, it includes several accumulation (construction) – abandonment (destruction) cycles on different spatial and temporal scales. On the sub-delta scale, four abandoned delta

lobes were formed within 43 years after 1934 AD (Huang et al., 1989), which have been investigated in the course of many studies of regional coastal dynamics, sedimentation and geomorphology (Peng et al., 2010; Yang et al., 2011; Bi et al., 2014; Wang et al., 2017; Wu et al., 2017; Zhan et al., 2020).

The study region lies within the warm temperate, semi-humid monsoon climate zone, with an annual average temperature of  $11.7\text{--}12.6^\circ\text{C}$  and annual precipitation of 530–630 mm, 70% of which is concentrated between June and September. The annual average wind speed in the modern YRD is 3.1–4.6 m/s, and gales ( $> 17\text{ m/s}$ ) are relatively frequent. During 1961–1980 there were 544 gales (671 days in total). The gales often cause strong wave action and storm surges, resulting in severe erosion of the abandoned delta coast. During the historical period the coastal area around the YRD was noted for strong storm surges. According to statistics in historical documents there were 31 disastrous storm surges in the Bohai Sea during the Little Ice Age, which was 10 times higher than the number during the Medieval Warm Period (Liu and Zhang, 1991). The frequent occurrence of these major storm surges during the Little Ice Age may have had a major impact on the geomorphic evolution of the abandoned YRD during the late abandonment stage (1482 AD–1855 AD). The Yellow River was the second-largest river in term of sediment load ( $1.08 \times 10^9\text{ t/yr}$ ) in the world (Milliman and Syvitski, 1992). Since the 1950s, the Yellow River sediments to the sea have decreased rapidly due to the human activities (Wang et al., 2007). During 2001–2010, the Yellow River annually has delivered  $23.5\text{ km}^3$  of water discharge and 149 Mt of sediment load to the sea, which is only  $\sim 14\%$  of the pre-1950s level (Hu et al., 2012). The estuarine tide is an irregular mixed semidiurnal tide with a mean tidal range of 1 m (0.6 m to 1.3 m). The tidal current is mainly dominated by reciprocating flows with a direction ranging from  $224^\circ$  to  $245^\circ$  and average velocity ranging from 29 cm/s to 37 cm/s at flood phase, and a direction ranging from  $49^\circ$  to  $78^\circ$  and average velocity ranging from 29 cm/s to 39 cm/s at ebb phase (Edition Committee of the Bay Chorography in China, 1993; Cheng and Gao, 2006).

## Materials and methods

### Sampling

Four boreholes (Table 1) were drilled in the study area in September 2018; their coordinates and elevations were obtained using TOPCON RTK, Japan. Single tube rotary drilling was used, with a coring tube diameter of 100 mm. The core sections were sealed and transported back to the laboratory, where they were split longitudinally, photographed and the lithology described. One half was then sampled at 5-cm intervals and the other half was sealed and stored in a freezer. The locations of samples for OSL dating were determined based on the lithology.

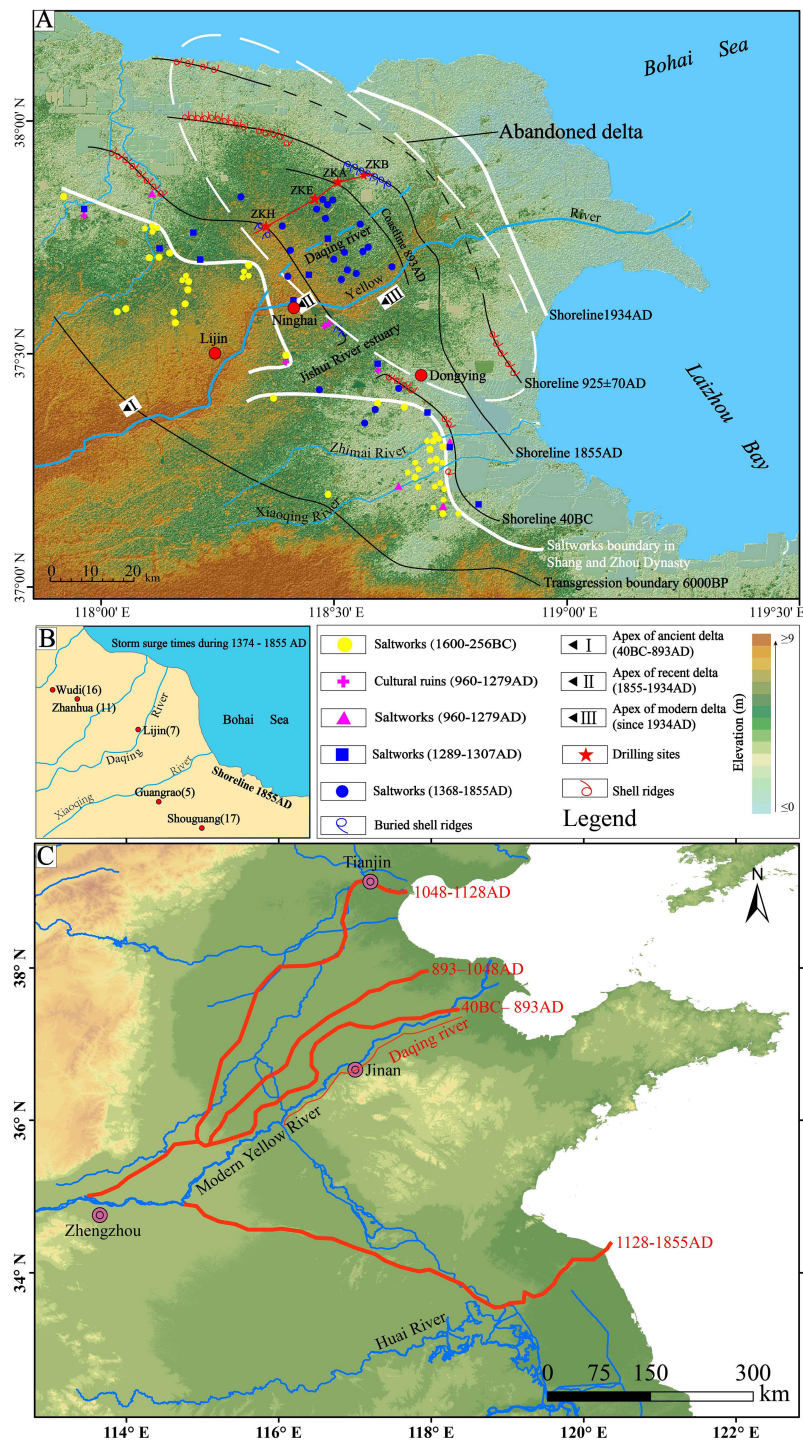


**FIGURE 1**  
**(A)** Geomorphic features of the Yellow River delta, including the shallow-buried abandoned delta, the spatiotemporal distribution of the ancient coastline, and the location of the sampling sites. **(B)** Location of the five cities during the Ming (1368 AD–1644 AD) and Qing (1636 AD–1912 AD) dynasties (Tan, 1975) and the number of storm surges during 1374–1855 AD (Wang, 2010). **(C)** The sketch map of changes in the course of the lower Yellow River during the last 2000 years (revised from Chen et al., 2012). Also shown are the distribution of ancient saltworks (Ji, 2009), with the coastal highlands on the inland side of the delta and more than 10 km away from the coastline in some areas.

TABLE 1 Location, elevation, depth and recovery for each borehole.

Core	Latitude	Longitude	Elevation (m)	Depth (m)	Recovery (%)
ZKH	37.75°N	118.35°E	4.22	14.80	90
ZKE	37.81°N	118.46°E	2.80	14.75	88
ZKA	37.85°N	118.51°E	1.82	13.40	99
ZKB	37.87°N	118.56°E	1.50	15.50	83

A total of 23 OSL samples and 996 samples for grain-size analysis were taken from the four cores.

## OSL dating

OSL samples were taken by hammering in metal tubes vertically into the core face, immediately after splitting. Layers with a high silt content were selected for sampling. The tubes were packed in black plastic bags and immediately sealed with adhesive tape to prevent light exposure and moisture loss. Sample preparation was conducted under subdued red light. The unexposed material in the central part of the tubes was wet sieved to extract the 38–63  $\mu\text{m}$  fraction, treated with 10% HCl and 30%  $\text{H}_2\text{O}_2$  to remove carbonates and organic matter, respectively, and then etched with 35%  $\text{H}_2\text{SiF}_6$  for two weeks to dissolve feldspars and then with 10% HCl to remove fluoride precipitates. The purity of the quartz grains was checked by infrared (IR,  $\lambda = 830 \text{ nm}$ ) stimulation. The isolated quartz grains were mounted as medium-sized (6 mm) aliquots in the centre of stainless steel discs using silicone oil.

The single-aliquot regenerative-dose (SAR) protocol (Murray and Wintle, 2000) was used for equivalent dose ( $D_e$ ) determination. The luminescence was stimulated by blue LEDs ( $\lambda = 470 \pm 20 \text{ nm}$ ) at  $130^\circ\text{C}$  for 40 s using a Risø TL/OSL-DA-20 reader with 90% diode power and was detected using a 7.5 mm-thick U-340 filter (detection window 275–390 nm) in front of the photomultiplier tube. Irradiations were carried out using a  $^{90}\text{Sr}/^{90}\text{Y}$  beta source in the reader. The preheat plateau test, dose recovery test, recuperation ratio and recycling ratio were analyzed on representative samples to select a suitable preheat temperature and to check the suitability of the SAR protocol.

In the current study, the concentrations of U, Th and K were measured by neutron activation analysis. The water content (mass of moisture/dry mass) was determined by weighing the sample before and after drying, with  $\pm 5\%$  uncertainties. The cosmic-ray dose rate was estimated for each sample as a function of depth, altitude and geomagnetic latitude (Prescott and Hutton, 1994). The dose rates and OSL ages were calculated by Dose Rate and Age Calculator (Durcan et al., 2015) and are listed in Table 2. In order to facilitate the comparison between sedimentary and historical records, the luminescence age (LA) in this paper can be converted into calendar age (CA) by the following method:  $\text{CA} = 2018 (\text{AD}) - 1000 * \text{LA} (\text{ka})$ ; If the

calculation result of CA is greater than zero, the calendar age use the notations AD, otherwise use BC.

## Grain-size analysis

Grain-size distributions were measured using a Malvern Mastersizer 3000 laser particle-size analyzer in the institute of coastal research of Ludong University, China. The pre-treatment procedure consisted of the removal of organic matter and carbonates by the addition of 10%  $\text{H}_2\text{O}_2$  and 10% HCl, respectively, followed by dispersal using 10 ml of 0.05 mol/L  $(\text{NaPO}_3)_6$  and treatment in an ultrasonic vibrator for 10 min (Lu and An, 1997).

## Results and discussion

### Sedimentary facies and stratigraphic architecture

The mean grain size ranges from silt (4–63  $\mu\text{m}$ ) to very fine sand (63–125  $\mu\text{m}$ ), with silt the dominant component in most samples. The down core clay content ( $<4 \mu\text{m}$ ) is relatively uniform, generally  $< 20\%$ , while the sand content (63–125  $\mu\text{m}$ ) shows the largest range of variation (0–90%). The sand layers rich in shell debris were found in boreholes cores ZKH (8–9m), ZKA (5.6–6.5m) and ZKB (3.7–4.2m), and the grain-size results also show that these layers mainly comprise very fine sand (Figures 2C–E). The grain-size depth profiles of the four borehole cores generally show two stages of variation. The lower part is generally coarser with a higher sandy component than in the upper part, reflecting a significant change in the sedimentary environment. The coarser sediments in the lower parts of the cores are mainly gray and dark gray, with cross bedding and wavy bedding (Figures 2H, I); while the sediments in the upper parts are mainly yellow silt without bedding structures (Figures 2A, B) and compacted silty clay (Figures 2F, G). According to the grain size, color and sedimentary structures of the sediments, the lower gray sediments may be delta-front facies, which are usually grayish or blackish due to reduction environment under the water; while the yellowish silts in the upper parts are possibly delta-plain facies, which are usually yellowish or brownish due to the oxidation environment formed by frequent exposure to air.

TABLE 2 OSL sample code, radionuclide concentrations, depth, water content and dose rates.

Sample no.	Burial depth (m)	U (ug/g)	Th (ug/g)	K (%)	Water content (%)	De (Gy)	Dose rate (Gy/ka)	Age (ka)
ZKA-1	4.62	2.82 ± 0.06	14.64 ± 1.91	2.01 ± 0.13	29	0.36 ± 0.09	3.01 ± 0.15	0.12 ± 0.03
ZKA-2	6.23	2.65 ± 0.04	12.58 ± 1.62	1.87 ± 0.11	24	2.76 ± 0.24	2.76 ± 0.13	1.00 ± 0.10
ZKA-3	6.58	2.15 ± 0.05	9.38 ± 1.12	1.63 ± 0.12	19	3.19 ± 0.16	2.28 ± 0.12	1.40 ± 0.10
ZKA-4	6.94	2.72 ± 0.06	13.45 ± 1.53	1.86 ± 0.11	19	4.20 ± 0.20	2.80 ± 0.13	1.50 ± 0.10
ZKA-5	12.62	2.32 ± 0.04	8.56 ± 1.14	1.52 ± 0.10	19	3.85 ± 0.61	2.14 ± 0.11	1.80 ± 0.30
ZKA-6	13.28	2.25 ± 0.05	7.93 ± 1.12	1.49 ± 0.09	24	3.92 ± 0.37	2.06 ± 0.10	1.90 ± 0.20
ZKE-1	4.22	2.77 ± 0.07	12.16 ± 1.49	1.53 ± 0.10	25	0.35 ± 0.05	2.49 ± 0.12	0.14 ± 0.02
ZKE-2	4.90	2.44 ± 0.05	12.39 ± 1.62	1.86 ± 0.12	23	0.43 ± 0.05	2.69 ± 0.13	0.16 ± 0.02
ZKE-3	6.23	2.19 ± 0.05	9.62 ± 1.25	1.51 ± 0.10	23	2.21 ± 0.19	2.21 ± 0.11	1.00 ± 0.10
ZKE-4	6.60	2.42 ± 0.05	12.34 ± 1.61	1.9 ± 0.12	24	4.70 ± 0.13	2.72 ± 0.14	1.73 ± 0.10
ZKE-5	7.42	2.36 ± 0.05	12.57 ± 1.63	1.95 ± 0.11	25	3.58 ± 0.21	2.76 ± 0.13	1.30 ± 0.10
ZKE-6	7.87	2.83 ± 0.05	8.92 ± 0.82	1.39 ± 0.09	22	3.92 ± 0.13	2.18 ± 0.10	1.80 ± 0.10
ZKE-7	11.30	1.97 ± 0.04	7.45 ± 0.84	1.51 ± 0.09	25	3.42 ± 0.37	2.01 ± 0.10	1.70 ± 0.20
ZKH-1	4.42	2.93 ± 0.07	9.85 ± 1.28	1.56 ± 0.10	22	0.36 ± 0.02	2.42 ± 0.11	0.15 ± 0.01
ZKH-2	4.89	2.95 ± 0.07	9.42 ± 1.23	1.63 ± 0.10	24	0.73 ± 0.09	2.44 ± 0.11	0.30 ± 0.04
ZKH-3	5.35	1.39 ± 0.03	6.43 ± 0.84	1.55 ± 0.10	25	3.28 ± 0.10	1.93 ± 0.10	1.70 ± 0.10
ZKH-4	7.56	2.93 ± 0.07	9.42 ± 1.21	1.67 ± 0.10	18	4.40 ± 0.44	2.44 ± 0.11	1.80 ± 0.20
ZKH-5	7.81	1.97 ± 0.04	9.07 ± 1.19	1.68 ± 0.10	19	4.37 ± 0.21	2.26 ± 0.11	1.94 ± 0.13
ZKH-6	9.24	1.89 ± 0.03	8.47 ± 0.84	1.54 ± 0.10	22	5.64 ± 0.57	2.09 ± 0.10	2.70 ± 0.30
ZKH-7	10.90	1.69 ± 0.04	7.52 ± 0.98	1.44 ± 0.09	19	1.93 ± 0.10	8.65 ± 0.35	4.49 ± 0.29
ZKB-1	3.65	2.37 ± 0.05	12.85 ± 1.69	1.83 ± 0.12	18	0.60 ± 0.08	2.72 ± 0.14	0.22 ± 0.03
ZKB-2	4.15	1.58 ± 0.04	11.32 ± 1.58	1.72 ± 0.11	26	1.52 ± 0.15	2.38 ± 0.12	0.64 ± 0.07
ZKB-3	4.58	2.43 ± 0.04	9.57 ± 0.84	1.52 ± 0.09	19	1.57 ± 0.12	2.27 ± 0.10	0.69 ± 0.06

The OSL dating results are listed in Table 2. Most of the samples show similar luminescence characteristics and normal distributions for the De values, suggesting that the medium-grained quartz (38–63 μm) was well bleached prior to deposition, which is consistent with a detailed study of the applicability of the OSL dating method to coastal sediments of the southern Bohai sea (Chen et al., 2013). Previous studies have shown that <sup>14</sup>C dating of coastal sediments is prone to age overestimation due to the carbon pool effect (Stanley and Chen, 2000); however, reliable late Holocene ages can be obtained using quartz OSL dating (Li et al., 2018). As shown in Figure 3, the OSL ages of the four boreholes generally change according to the stratigraphic depth sequence, with the age range of 0.12–4.60 ka. Based on the OSL ages and depth changes in sedimentary facies, the stratigraphy of the four boreholes can be sub-divided and correlated, as shown in Figure 4. The sequences can be divided into four sedimentary units according to the isochronic planes of the OSL dating and the major stages of delta development recorded by the historical documents (Gao et al., 1989): Holocene transgressive strata (Before 40 BC), the ancient delta (40 BC–893 AD), the abandoned delta (893 AD–1855 AD), and the modern delta (1855 AD to present). The sand layers within the cores, combined with the OSL chronology, could be used to determine the location of the coastline at various times as

one of the evidences: in 40 BC (ZKH), 893 AD (ZKA), and 1855 AD (ZKB).

## Geomorphic features of the shallow-buried abandoned Yellow River delta

The spatiotemporal distribution of the former coastline of the YRD since 40 BC, when the Yellow River captured the Jishui River channel, has been reconstructed using various forms of evidence: sand layers containing shell fragments in three of the boreholes (Figure 4), the distribution of saltworks during the historical period (Figure 1A), ancient shell beach ridges and buried shell beach ridges (Figure 1A), and the results of previous studies (Guo, 1980; Zhuang et al., 1991; Ji, 2009). The coastlines of 40 BC and 925 AD were determined based on topography, borehole data (including the sand layers with shell fragments in core ZKH), and the <sup>14</sup>C ages of ancient shell ridges (Zhuang et al., 1991). The coastline of 893 AD was determined based on sand layers with shell fragments in core ZKA. The coastlines of 1855 AD and 1934 AD and the modern YRD were determined based on the results of Guo (1980), together with field investigations and the borehole core data (including the sand layers with shell fragments in core ZKB). The results show that

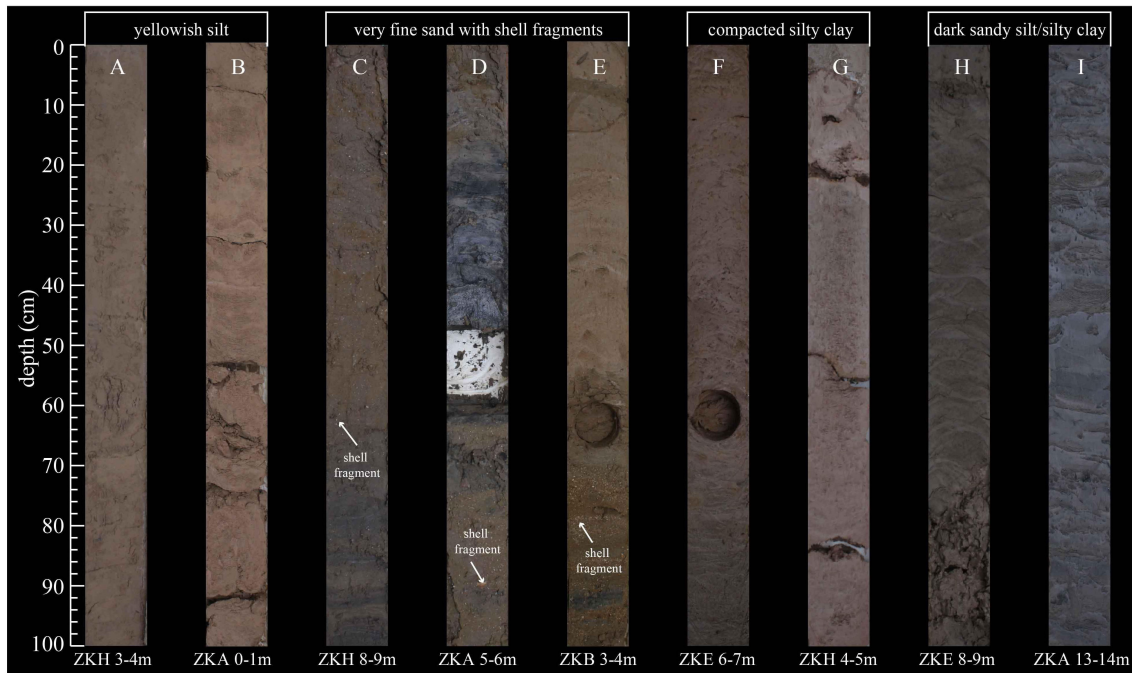


**FIGURE 2**  
 Photographs of representative sedimentary facies of the drilling cores. (A, B) delta plain; (C–E) beach ridge; (F, G) abandoned delta plain; (H, I) delta front. The circles in the ZKB 3–4 m (E) and ZKE 5–7 m (F) are the sampling position of OSL dating.

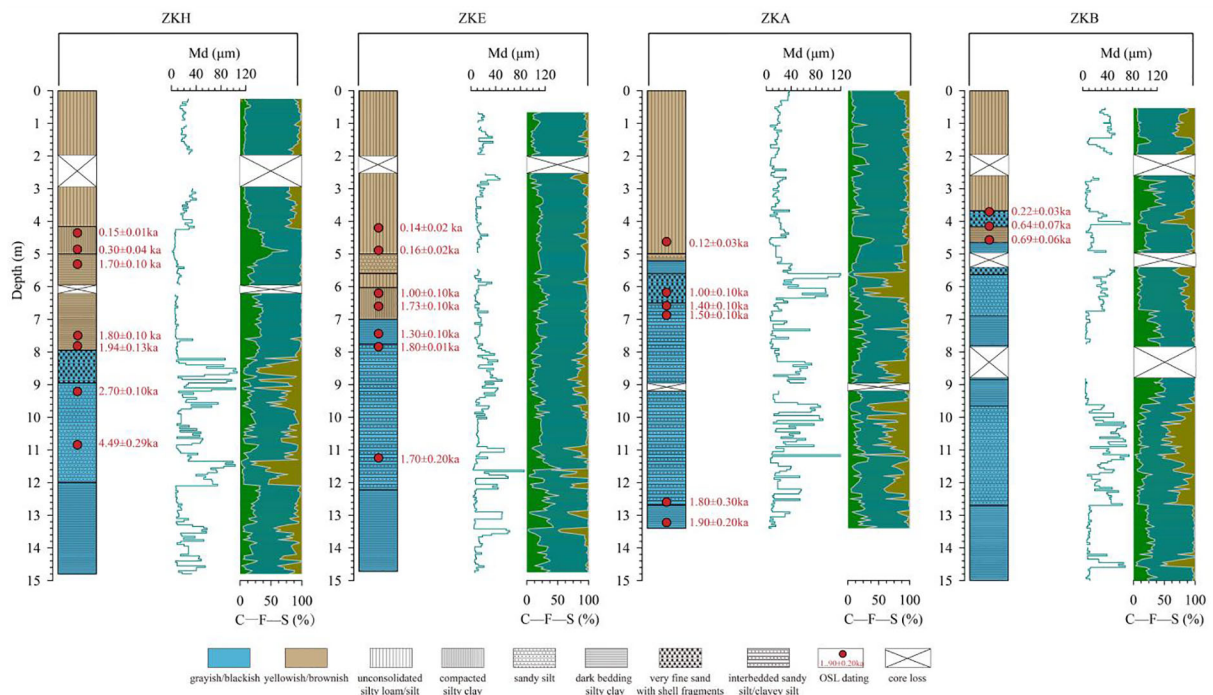


**FIGURE 3**  
 Profiles of lithology and selected grain size parameters for the four drilling cores. The OSL ages are also shown. Mz: mean grain size; C→F→S: the contents of clay, silt and sand, respectively.

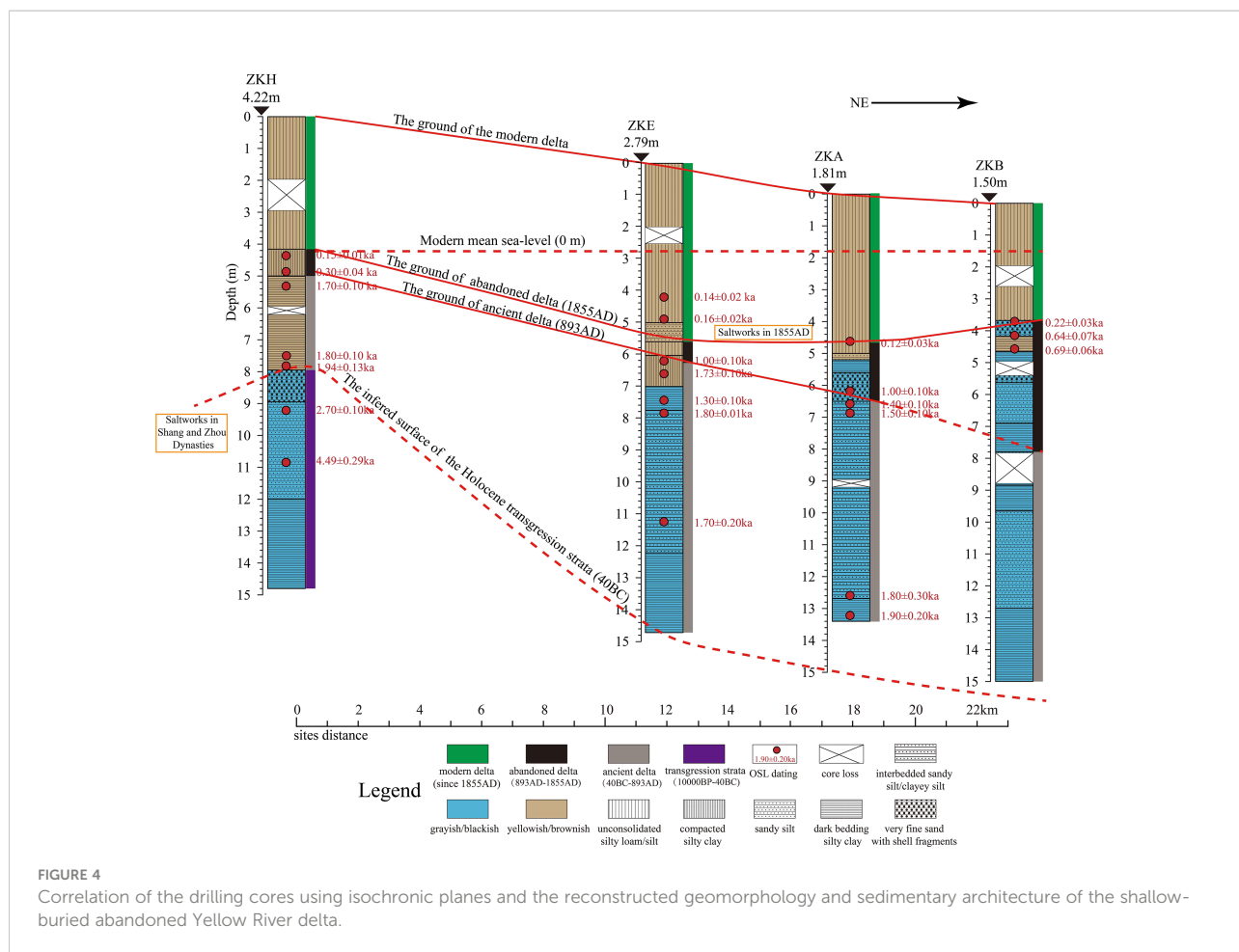


**FIGURE 4**  
Correlation of the drilling cores using isochronic planes and the reconstructed geomorphology and sedimentary architecture of the shallow-buried abandoned Yellow River delta.

the abandoned Yellow River delta was mainly distributed in the central plain of the Yellow River delta between the 1934 AD coastline and the saltworks pre-dating the Qin dynasty (Before 256 BC). As shown in Figure 1A, the four boreholes constitute a cross section from land to sea. The cross section is parallel to the left bank of the Daqing River, which is roughly located along the axis of the shallow-buried abandoned YRD and spans the three coastlines of 40 BC, 893 AD, and 1855 AD. The spatiotemporal distribution of sediment deposition recorded by the boreholes reveals that the shallow-buried abandoned delta has the following three geographic features:

(1) Inverse terrain gradient from land to sea

As shown in Figure 4, in 893 AD, when the delta was abandoned, the elevation of the terrain of the ancient delta decreased from southwest to northeast; and in 1855 AD, before its burial, elevation of the delta decreased and then increased from southwest to northeast. The abandoned delta deposits abruptly become thicker from southwest to northeast, showing a slender horn-shape. The OSL age of the highlands on the seaward side of the delta is 1019–1799 AD (1–0.22 ka), and that of the main body is 1379–1799 AD (0.64–0.22 ka). Therefore, different from the pattern of the terrain of the modern YRD,

which has an elevated long axis (containing the river channel) and lower sides, with higher elevations upstream and lower elevations downstream. It was also different from the ancient delta of 893 AD that dipped gradually from land to sea, with the elevation of the terrain of the abandoned delta high on both sides and low in the middle, along the northeast-southwest direction, with height differences of ~3.3 m and ~1.0 m, respectively. The slopes of the southwest and northeast parts are 2.03 ‰ and 1.44 ‰, which are respectively ~3 times and ~2 times greater than the slope of the modern deltaic plain (0.75 ‰) (Figure 4). The northeast side is a low and gently sloping coastal highland distributed along the 1855 AD coastline, which is located between the 925 AD and 893 AD coastlines, with a width of ~20 km. The top of the highland is ~1.01 m higher than the lowest part of the depression, and ~2.59 m higher than the top of the 893 AD beach sediment layer in the ZKA borehole, forming an inverse gradient from the plain depression to the coastal highland in the SW–NE direction (Figures 1, 4).

Previous studies have shown that in the five counties of the YRD during the Ming and Qing dynasties, Lijin and Guangrao, which were along the long axis of the delta, experienced seven and five severe storm surges, respectively, during 1374 AD–1855

AD. This was much lower than at Wudi (16) on the west side, and at Zhanhua (11) and Shouguang (17) on the east side (Wang, 2010). However, the landward part of the coastal highland was a sea salt-producing area for more than 500 years (1289–1855 AD) in the middle and late stages of the abandoned delta (Figure 1). Before the 16th century, salt in the YRD was produced using topsoil with a high salt content and shallow underground brine as raw materials, rather than directly using seawater (Ji, 2009). This indicates that before 1855 AD there was a large-scale positive terrain barrier along the coast of the abandoned delta and a shallow-buried high concentration of underground brine in the landward plain.

### (2) Sandy coast and deep estuarine channel

The 40 BC and 1855 AD coastlines in the central plain of the YRD demarcate the land-sea boundary before the ancient delta formed and before the abandoned delta was buried, respectively (Figure 1). However, there are two shorelines corresponding to the ancient delta when it was abandoned. The age of the first is 893 AD, while the  $^{14}\text{C}$  age of the lower shell ridges of the second is  $925 \pm 70$  AD (Chen, 1982), with the intervening distance of  $\sim 20$  km (Figure 1). Considering the possible error in the  $^{14}\text{C}$  dating results and that the  $^{14}\text{C}$  age of the other site of the younger shoreline is  $835 \pm 90$  AD (Chen, 1982), it can be determined that the geomorphic ages of the two coastlines are the same. Therefore, at the beginning of the formation of the abandoned delta there was a compound coast, and offshore shell ridges were developed 20 km away from the continental coastline (Figure 5C). A low-energy sedimentary environment of coastal shallow lakes and marshes was developed between the ridges and the land, which subsequently evolved into the above mentioned low elevation and gently sloping highland, and a single sandy coast developed outside the highland.

After the Yellow River captured the Jishui River and entered the sea in 40 BC, the middle and lower reaches of the ancient Jishui River gradually evolved into the Daqing River, entering the sea along the southern depression of the ancient delta. After 1077 AD, the lower reach of the Daqing shifted northeastward towards the sea *via* Lijin, incising the abandoned delta and forming a new estuary (Figure 1). The estuary of the Daqing River is 15–20 m deep with the abandoned delta plain as its first terrace, which is 6–9 m higher than the low-water level. The channel is a single rectangular section 30 m wide and 6–9 m deep, with the tidal boundary being above Lijin (Gao et al., 1989). Given the earliest establishment of Tiemenguan wharf in the Jin Dynasty (1115–1234 AD), shortly after 1128 AD, it can be inferred that the abandoned delta was incised after the diversion of the Daqing River. Subsequently, a single, meandering, rectangular-shaped deep estuary gradually formed. Until 1855 AD, it was an important port for salt transport, but shortly after 1855 AD it became silted up, abandoned and eventually buried.

### (3) Depth of sediment accumulation

In addition to the incised landform of the estuary channel of the Daqinghe River, the abandoned delta plain is an

accumulation geomorphic body stacked on top of the ancient delta. However, the sediment types, thickness and the sequence of the different geomorphic components vary substantially (Figure 4). The thickness of the coastal highland after abandonment exceeds 4.0 m. The protruding part is 1.5–2.0 m-thick with abundant shell fragments and thin silt layers belonging to lake-marsh facies. The silt is black or dark gray in color with a high organic matter content; it changes gradually upward to grayish yellow continental silty clay or clayey silty sand (Figure 3). The OSL chronology for the upper part of the ZKB and ZKA boreholes shows that the sedimentary ages at the base and top of the highland are  $1019 \pm 100$  AD and  $1799 \pm 30$  AD, respectively. The former age is later than the formation of the abandoned delta, and the latter age is earlier than the burial of the abandoned delta. The protruding part of the highland recorded in the ZKB borehole was formed during  $1379 \pm 60$  to  $1799 \pm 30$  AD, in the late stage of delta abandonment.

The abandoned delta in the plain depression accumulated a  $\sim 0.5$ – $1.0$  m-thickness of continental silty clay sediments with a sediment deposition rate less than that of the northeastern coastal highland, and also less than that of the overlying modern delta and the underlying ancient delta. According to the chronology of the ZKH borehole core, on the west side, the average deposition rate of the plain depression is only 0.87 mm/yr; the rate for the modern delta is 25.37 mm/yr, that for the ancient delta is 5.31 mm/yr, and that for the highland ZKB borehole core during the same period is 4.38 mm/yr (Figure 3). The sediments for almost the whole of the ZKH borehole core and the lower part of the ZKE borehole core in this layer are compact, with brownish-red and brownish-yellow colors and a low sand content (Figures 2F, G). Additionally, they contain numerous black carbon fragments or horizontal carbon bands, and a small amount of Fe-Mn rust spots, termed the “laterite layer” by local villagers during well digging. This indicates that the vertical aggradation of the abandoned delta plain was slow and pedogenesis relatively strong.

## Major geomorphic processes and a model of the evolution of the shallow-buried abandoned Yellow River delta

The period between the emergence of the abandoned delta and its burial was  $\sim 1000$  years (893AD–1855 AD), spanning the interval from the Medieval Warm Period to the Little Ice Age, when there were major changes in geomorphic processes, including a reduction in the sediment supply, and changes in storm surge intensity. These changes are discussed below.

### (1) Reduction in sediment supply

Delta construction is the result of the input, transportation and accumulation of river sediment, and changes in the river estuary will inevitably have a profound effect on the geomorphic evolution of an abandoned delta (Peng et al., 2010). After 893

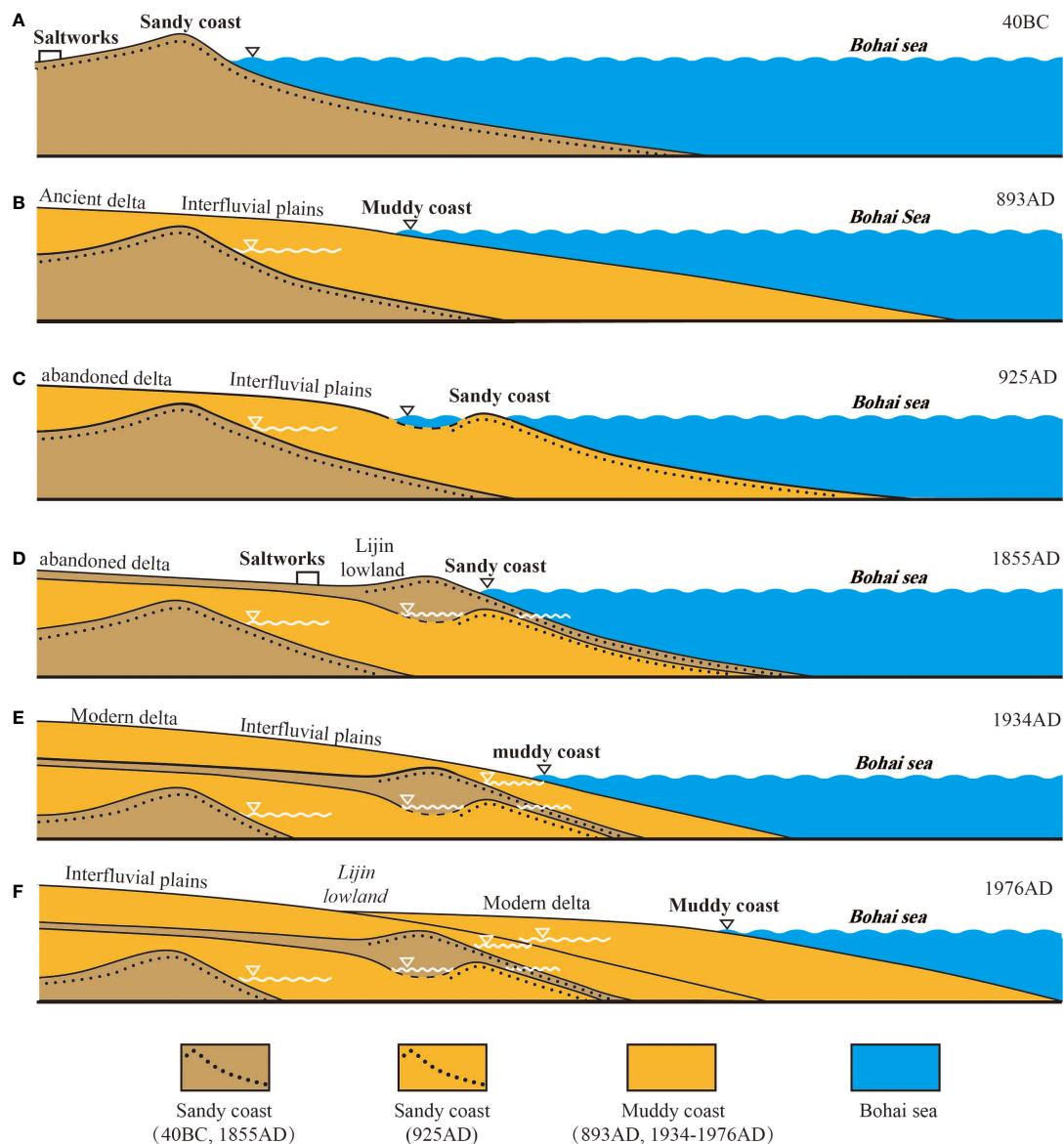


FIGURE 5

Model of the geomorphic evolution of the shallow-buried abandoned Yellow River delta during the last 2000 years. (A) The sandy coast was developed before the ancient Yellow River Delta was formed in 40 BC. (B) The muddy coast was developed before the abandonment of the ancient Yellow River Delta in 893 AD. (C) The muddy coast was transformed into a sandy coast and offshore shell ridges were formed beyond the continental coastline in 925 AD. (D) The sandy coast was developed before the abandoned delta buried by sediments of the Yellow River in 1855 AD. (E) The sandy coast was transformed into muddy coast after 1855 AD. (F) The modern delta deposits prograde and rapidly advance the muddy coast into the sea.

AD the Yellow River changed its course from the ancient YRD, entering the Bohai Sea to the north of the abandoned delta (Guo, 1980). After 1128 AD most of the runoff and sediment flowed southward, capturing the channel of the Huai River to the South Yellow Sea. After 1495 AD all of the water and sediment load of the Yellow River entered the South Yellow Sea via the Huai River; previously, only a small amount of water and sediment entered the sea via Lijin. During this period, at ~1077 AD, the

Daqing River (It originated from the Shandong province) flowed into the Bohai Sea through the abandoned delta via Lijin, forming a new estuary (Chen, 1982). Therefore, during the intervals of 893–1077 AD, 1077–1128 AD, 1128–1495 AD and 1495–1855 AD, the runoff and sediment supply to the abandoned delta underwent major changes. The influence of the Yellow River on the abandoned delta gradually weakened, and after 1495 AD it ceased completely, leaving the abandoned

delta affected solely by the erosive estuary of the Daqing River, which has a much lower sediment load (Chen, 1982). Therefore, the existence of shell ridges and sand layers with shell fragments in the borehole cores indicates that, with the reduction of sediment supply from the Yellow River, the effects of wave erosion on the abandoned YRD increased, transforming the ancient delta from a muddy coast to a sandy coast.

## (2) Changes in climate and storm surges

Changes in climate, storm surges and wave activity substantially affect coastal environments and hence the geomorphic evolution of coastal estuaries and deltas (Yang et al., 2019). Speleothem  $\delta^{18}\text{O}$  and  $\delta^{13}\text{C}$  records from Kaiyuan cave, 150 km southwest of Lijin, provide a regional climatic record during 892–1894 AD (Wang et al., 2015). The 590 years before 1482 AD comprised the Medieval Warm Period (MWP) when the summer monsoons was strong and stable, and the 412 years after 1482 AD comprised the Little Ice Age (LIA) when the summer monsoon was weak and unstable (Figure 6). Strong storm surges prevailed around the Bohai Sea during the past 2000 years (Feng, 1982; Liu, 1989). Based on the observing hydrodynamic and sediment data, the simulation results of an abandoned Yellow River Delta lobe, revealed that local storms enhanced tidal residual currents and considerably weakened tidal shear front, intensified the sediment resuspension and dispersal (Fan et al., 2020). Under storm conditions, surface suspended sediment concentration was 2 times as large as that in normal conditions. Moreover, the weakened tidal shear front was in favour of the sediment dispersal in the river mouth and southward diffuses to the central area of the Laizhou Bay (Fu et al., 2021). Laizhou Bay, where the modern YRD is located, experiences a storm surge once every three years on average during the recent 50 years; during intervals of strong wind and wave action, the storm surge height increases by 2.11–5.74 m and lasts for 24–72 hr (Wang et al., 2016), providing energy and an accumulation space for coastal landform development. According to statistics from historical documents (Liu and

Zhang, 1991), there were nine storm surge disasters in the ancient delta area of the Bohai Sea during the interval of 933 years (40BC–893AD), but as many as 34 storm surges affected the abandoned delta during the interval of 962 years (893AD–1855AD). During the 962 years of the abandoned delta, for the 589 years prior to 1482 AD there were only 3 storm surges, while in the 373 years after 1482 AD there were as many as 31 (Figure 6). As shown in Figure 1, the 1855 AD coastline is located on the landward side of the  $925 \pm 70$  AD coastline, indicating that the abandoned delta had migrated inland in the late abandonment stage, forming a coastal highland. Therefore, the frequent and intense storm surge activity after 1482 AD, during the Little Ice Age, may have promoted the formation of the coastal highland–depression system of the abandoned delta.

Based on the foregoing analysis of the processes affecting the evolution of the YRD, combined with the sedimentary evidence from the borehole cores and the results of previous studies (Guo, 1980; Zhuang et al., 1991), the geomorphic evolution of the shallow-buried abandoned YRD during 893–1855 AD (Figure 5) was reconstructed. These evolutionary stages are summarized below.

- i. After the ancient YRD (40 BC–893 AD) was abandoned due to the reduction in sediment supply in 893 AD, the existing muddy coast was transformed to a sandy coast under the influence of wave erosion, and offshore shell ridges were formed beyond the continental coastline.
- ii. During the abandonment stage (893–1855 AD) and especially during the Little Ice Age after 1482 AD, driven by storm surges, the shell ridges migrated laterally, widened and increased rose, while sediment accumulation on the landward-side interfluvial floodplains was relatively weak. This configuration constituted the coastal highland–plain depression system. After 1077 AD the Daqing River flowed into the Bohai Sea through the abandoned delta *via* Lijin,

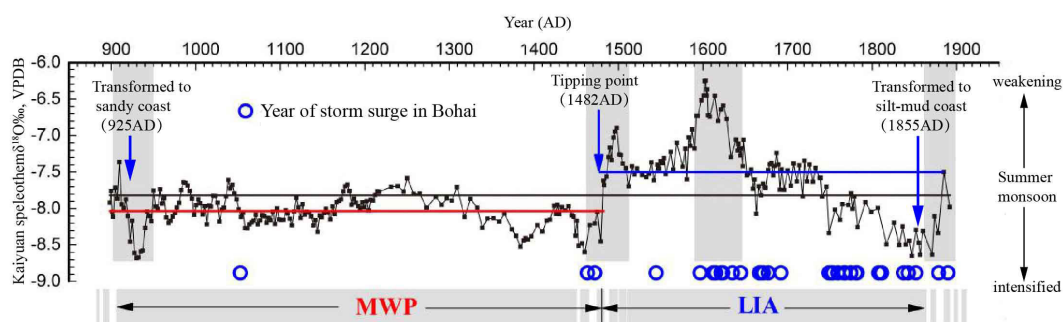


FIGURE 6  
 $\delta^{18}\text{O}$  record from Kaiyuan cave (Wang et al., 2015), showing changes in summer monsoon intensity during 892–1894 AD and the occurrence of storm surges in the Bohai Sea (Liu and Zhang, 1991). The four vertical gray bars indicate the abrupt climatic events.

forming a new estuary. The coastal highland–plain depression system and the abandoned delta were jointly eroded by the estuary of the Daqing River.

iii.

After 1855 AD the abandoned delta landform system was completely buried by sediments of the Yellow River, and the wave-controlled sandy coast was transformed to a tide-controlled silty-mud coast.

In brief, after the reduction in sediment supply in 893 AD, the simplex muddy coast was transformed to a compound sandy coast. The coast did not retreat significantly, but the topographic relief increased and the slope became steep. The large-scale ancient deltas, which first developed some 2000 years ago, were rapidly abandoned some 1000 years ago. They were then exposed during the interval from the Medieval Warm Period to the Little Ice Age and then rapidly buried to a shallow depth. This process was accompanied by significant changes in estuary types, which were unique amongst river deltas on a global scale. Their geomorphic characteristics were completely different from those of the modern Yellow River and the abandoned YRD in northern Jiangsu, and they also differed from those of the Luan River delta in the northern Bohai Sea (Xu et al., 2020) and the ancient estuary lagoon coast in the southern part of Laizhou Bay (Han et al., 2002). They differed from the classical sandbar-lagoon system but also differed from the abandoned (sub-) deltas of other major rivers.

## Conclusions

We have used analyses of grain-size and sedimentary facies and OSL dating of four borehole cores, combined with an analysis of landform morphology, to reconstruct the geomorphic evolution of the ancient abandoned YRD during the interval of its emergence. The spatiotemporal distribution of sediment deposition recorded by the boreholes reveals that the shallow-buried abandoned delta has the following three geomorphic features: 1) inverse terrain gradient from land to sea; 2) sandy coast and deep estuarine channel; 2) the vertical aggradation. Reduction in sediment supply, together with changes in climate and storm surges, have led to the geomorphic evolution of the ancient abandoned YRD. After the ancient YRD was abandoned in 893 AD due to the reduction in the sediment supply, a sandy coast controlled by wave action was formed, together with offshore shell ridges seaward of the continental coastline. During the interval from the Medieval Warm Period to the Little Ice Age, driven by storm surges, the shell ridges migrated laterally, widened and rose, while sediment accumulation in the landward-side interfluvial floodplains was relatively weak. These components constituted the coastal highland–plain depression system, which replaced the previous

island–land sandbar-lagoon system, which is unique among major river deltas.

## Data availability statement

The original contributions presented in the study are included in the article. Further inquiries can be directed to the corresponding authors.

## Author contributions

QW and CZ designed the research. LZ and XL analyzed the chronology and sedimentary sequences of the drilling cores. XL analyzed the grain-size data. QW, LZ, CZ and XL wrote the manuscript, which was edited by all of the co-authors. LW, SC and BC refined the interpretations. All authors reviewed the manuscript. All authors contributed to the article and approved the submitted version.

## Funding

We are grateful for financial support from the National Science Foundation of China – Shandong United fund (U1706220), the National Natural Science Foundation of China (41901006, 41901102), and the Youth Innovation and Technology Program Team of Shandong University (2020KJH002).

## Acknowledgments

We thank Cheng Dong and Feng Yin for their help with field sampling.

## Conflict of interest

The authors declare that the research was conducted in the absence of any commercial or financial relationships that could be construed as a potential conflict of interest.

## Publisher's note

All claims expressed in this article are solely those of the authors and do not necessarily represent those of their affiliated organizations, or those of the publisher, the editors and the reviewers. Any product that may be evaluated in this article, or claim that may be made by its manufacturer, is not guaranteed or endorsed by the publisher.

## References

- Bacino, G. L., Dragani, W. C., and Codignotto, J. O. (2019). Changes in wave climate and its impact on the coastal erosion in samborombón bay, río de la plata estuary, Argentina. *Estuar. Coast. Shelf S* 219, 71–80. doi: 10.1016/j.jce.2019.01.011
- Bi, N., Wang, H., and Yang, Z. (2014). Recent changes in the erosion–accretion patterns of the active huanghe (Yellow river) delta lobe caused by human activities. *Cont. Shelf Res.* 90, 70–78. doi: 10.1016/j.csr.2014.02.014
- Brooks, S. M., Spencer, T., and Christie, E. K. (2017). Storm impacts and shoreline recovery: Mechanisms and controls in the southern north Sea. *Geomorphology* 283, 48–60. doi: 10.1016/j.geomorph.2017.01.007
- Burvingt, O., Masselink, G., Scott, T., Davidson, M., and Russell, P. (2018). Climate forcing of regionally-coherent extreme storm impact and recovery on embayed beaches. *Mar. Geol.* 401, 112–128. doi: 10.1016/j.margeo.2018.04.004
- Chamberlain, E. L., Törnqvist, T. E., Shen, Z., Mauz, B., and Wallinga, J. (2018). Anatomy of Mississippi delta growth and its implications for coastal restoration. *Sci. Adv.* 4, eaar4740. doi: 10.1126/sciadv.aar4740
- Chen, J. (1980). *The coastal geomorphology. editorial board of physical geography of China, physical geography of China (geomorphology)* (Beijing: the Science Publishing Company).
- Chen, J. (1982). *The historical changes of bohai bay coast. editorial board of physical geography of China, physical geography of China (historical physical geography)* (Beijing: the Science Publishing Company).
- Cheng, Y. J., and Gao, J. (2006). Analysis of hydrographic characteristics and changes in scour and silting in the laizhou bay area. *Coast. Eng.* 25 (3), 1–6. doi: 10.3969/j.issn.1002-3682.2006.03.001
- Chen, Y., Syvitski, J., Gao, S., Overeem, I., and Kettner, A. (2012). Socio-economic impacts on flooding: A 4000-year history of the yellow river, China. *AMBIO* 41 (7), 682–698. doi: 10.1007/s13280-012-0290-5
- Chen, G., Yi, L., Xu, X., Yu, H., Cao, J., Su, Q., et al (2013). Testing the standardized growth curve (SGC) to OSL dating coastal sediments from the south Bohai Sea, China. *Geochronometria* 40 (2), 101–112. doi: 10.2478/s13386-013-0103-z
- Dai, Z., Liu, J., Wei, W., and Chen, J. (2014). Detection of the three gorges dam influence on the changjiang (Yangtze river) submerged delta. *Sci. Rep.* 4, 6600. doi: 10.1038/srep06600
- Dai, Z., Mei, X., Darby, S.E., Lou, Y., and Li, W. (2018). Fluvial sediment transfer in the Changjiang (Yangtze) river–estuary depositional system. *J. Hydrol.* 566, 719–734. doi: 10.1016/j.jhydrol.2018.09.019
- Durcan, J. A., King, G. E., and Duller, G. A. T. (2015). DRAC: Dose rate and age calculator for trapped charge dating. *Quat. Geochronol.* 28, 54–61. doi: 10.1016/j.quageo.2015.03.012
- Edition Committee of the Bay Chorography in China (1993). *The bay chorography in China* Vol. 3) (Beijing: Ocean Press), 1–81.
- Eisemann, E. R., Wallace, D. J., Buijsman, M. C., and Pierce, T. (2018). Response of a vulnerable barrier island to multi-year storm impacts: LiDAR-data-inferred morphodynamic changes on ship island, Mississippi, USA. *Geomorphology* 313, 58–71. doi: 10.1016/j.geomorph.2018.04.001
- Fan, Y. S., Chen, S. L., Pan, S., and Dou, S. T. (2020). Storm-induced hydrodynamic changes and seabed erosion in the littoral zone of yellow river delta: A model-guided mechanism study. *Cont. Shelf Res.* 205, 104171. doi: 10.1016/j.csr.2020.104171
- Feng, S. (1982). *Introduction to storm surge* (Beijing: the Science Publishing Company).
- FitzGerald, D. M., Fenster, M. S., Argow, B. A., and Buynevich, L. V. (2008). Coastal impacts due to sea-level rise. *Annu. Rev. Earth Pl. Sc.* 36, 601–647. doi: 10.1146/annurev.earth.35.031306.140139
- Fu, Y. T., Chen, S. L., Ji, H. Y., Fan, Y. S., and Li, P. (2021). The modern yellow river delta in transition: Causes and implications. *Mar. Geol.* 436, 106476. doi: 10.1016/j.margeo.2021.106476
- Ganti, V., Chadwick, A. J., Hassenruck-Gudipati, H. J., and Lamb, M. P. (2016). Avulsion cycles and their stratigraphic signature on an experimental backwater-controlled delta. *J. Geophys. Res-Earth* 121 (9), 1651–1675. doi: 10.1002/2016JF003915
- Gao, S., Li, Y., An, F., Wang, Y., and Yan, F. (1989). *Formation and sedimentary environment of the yellow river delta* (Beijing: the Science Publishing Company).
- Gao, L., Long, H., Zhang, P., Tamura, T., Feng, W., and Mei, Q. (2019). The sedimentary evolution of Yangtze river delta since MIS3: A new chronology evidence revealed by OSL dating. *Quat. Geochronol.* 49, 153–158. doi: 10.1016/j.quageo.2018.03.010
- Giosan, L., Donnelly, J. P., Vespremeanu, E., Bhattacharya, J. P., Olariu, C., and Buonaiuto, F. S. (2005). River delta morphodynamics: examples from the Danube delta. *SEPM Spec. Publ.* 83, 393–411. doi: 10.2110 pec.05.83.0393
- Gopikrishna, B., and Deo, M. (2018). Changes in the shoreline at paradip port, India in response to climate change. *Geomorphology* 303, 243–255. doi: 10.1016/j.geomorph.2017.12.012
- Gugliotta, M., and Saito, Y. (2019). Matching trends in channel width, sinuosity, and depth along the fluvial to marine transition zone of tide-dominated river deltas: The need for a revision of depositional and hydraulic models. *Earth-Sci. Rev.* 191, 93–113. doi: 10.1016/j.earscirev.2019.02.002
- Guo, Y. (1980). Coastal changes in the yellow river delta in modern times. *Mar. Sci.* 1, 33–37.
- Han, M., Zhang, W., Li, Y., and Zhang, L. (2002). Formation and change of ancient lake on south coast plain of laizhou bay. *Sci. Geogr. Sinica.* 4), 430–435. doi: 10.13249/j.cnki.sgs.2002.04.430
- Hoitink, A. J. F., Wang, Z. B., Vermeulen, B., Huismans, Y., and Kästner, K. (2017). Tidal controls on river delta morphology. *Nat. Geosci.* 10 (9), 637–645. doi: 10.1038/ngeo3000
- Houser, C., Hapke, C., and Hamilton, S. (2008). Controls on coastal dune morphology, shoreline erosion and barrier island response to extreme storms. *Geomorphology* 100 (3–4), 223–240. doi: 10.1016/j.geomorph.2007.12.007
- Hu, B., Li, G., Li, J., Bi, J., Zhao, J., and Bu, R. (2012). Provenance and climate change inferred from Sr-Nd-Pb isotopes of late quaternary sediments in the huanghe (Yellow river) delta, China. *Quaternary Res.* 78, 561–571. doi: 10.1016/j.yqres.2012.07.005
- Huang, S., Li, Y., An, F., Wang, Y., and Yan, F. (1989). *Formation and sedimentary environment of the Yellow River Delta.* (Beijing: the Science Publishing Company).
- Janssen-Stelder, B. (2000). The effect of different hydrodynamic conditions on the morphodynamics of a tidal mudflat in the Dutch wadden Sea. *Cont. Shelf Res.* 20 (12–13), 1461–1478. doi: 10.1016/S0278-4343(00)00032-7
- Jerolmack, D. J., and Mohrig, D. (2007). Conditions for branching in depositional rivers. *Geology* 35 (5), 463–466. doi: 10.1130/G23308A.1
- Ji, L. (2009). *Research on Shandong salt industry in Ming and Qing dynasties* (Jinan: Qilu Publishing House).
- Jiang, C., Pan, S., and Chen, S. (2017). Recent morphological changes of the yellow river (Huanghe) submerged delta: Causes and environmental implications. *Geomorphology* 293, 93–107. doi: 10.1016/j.geomorph.2017.04.036
- Koiwa, N., Takahashi, M., Sugisawa, S., Ito, A., Matsumoto, H., Tanavud, C., et al. (2018). Barrier spit recovery following the 2004 Indian ocean tsunami at pakarang cape, southwest Thailand. *Geomorphology* 306, 314–324. doi: 10.1016/j.geomorph.2017.05.003
- Li, H., Li, Y., Zheng, B., Zhong, G., Zhang, H., Wang, H., et al. (2019). Typhoon soudelor, (2015) induced offshore movement of sand dunes and geomorphological change: Fujian coast, China. *Water-Sui* 11 (6), 1191. doi: 10.3390/w11061191
- Li, Y., Shang, Z., Tsukamoto, S., Tamura, T., Yi, L., Wang, H., et al. (2018). Quartz and K-feldspar luminescence dating of sedimentation in the north bohai coastal area (NE China) since the late pleistocene. *J. Asian Earth Sci.* 152, 103–115. doi: 10.1016/j.jseaes.2017.10.036
- Liu, A. (1989). On the historical storm surges along the Shandong coast. *J. Ocean Univ. QingDao* 19 (3), 22–30. doi: 10.16441/j.cnki.hdx.1989.03.003
- Liu, A., and Zhang, D. (1991). On the historical storm surges round the bohai Sea region. *J. Ocean Univ. QingDao* 21 (2), 21–36. doi: 10.16441/j.cnki.hdx.1991.02.003
- Lu, H. Y., and An, Z. S. (1997). Pretreated methods on loess-palaeosol samples granulometry. *Chin. Sci. Bull.* 43, 237–240. doi: 10.1007/BF02898920
- Milliman, J. D., and Syvitski, J. P. M. (1992). Geomorphic/tectonic control of sediment discharge to the ocean: The importance of small mountainous rivers. *J. Geol.* 100, 525–544. doi: 10.1086/629606
- Murray, A. S., and Wintle, A. G. (2000). Luminescence dating of quartz using an improved single-aliquot regenerative-dose protocol. *Radiat. Meas.* 32, 57–73. doi: 10.1016/S1350-4487(99)00253-X
- Nienhuis, J. H., Ashton, A. D., Roos, P. C., Hulscher, S. J., and Giosan, L. (2013). Wave reworking of abandoned deltas. *Geophys. Res. Lett.* 40 (22), 5899–5903. doi: 10.1002/2013GL058231
- Ning, W., Nielsen, A. B., Ivarsson, L. N., Jilbert, T., Åkesson, C., Slomp, C. P., et al. (2018). Anthropogenic and climatic impacts on a coastal environment in the Baltic Sea over the last 1000 years. *Anthropocene* 21, 66–79. doi: 10.1016/j.anucene.2018.02.003
- Peng, J., Chen, S., and Dong, P. (2010). Temporal variation of sediment load in the yellow river basin, China, and its impacts on the lower reaches and the river delta. *Catena* 83 (2–3), 135–147. doi: 10.1016/j.catena.2010.08.006

- Phillips, J. D., Slattery, M. C., and Musselman, Z. A. (2004). Dam-to-delta sediment inputs and storage in the lower trinity river, Texas. *Geomorphology* 62 (1–2), 17–34. doi: 10.1016/j.geomorph.2004.02.004
- Pryor, S. C., and Barthelmie, R. (2010). Climate change impacts on wind energy: A review. *Renew. Sust. Energ. Rev.* 14 (1), 430–437. doi: 10.1016/j.rser.2009.07.028
- Prescott, J., and Hutton, J. (1994). Cosmic ray contributions to dose rates for luminescence and ESR dating: Large depths and long-term time variations. *Radiat. Meas* 23 (2–3), 497–500. doi: 10.1016/1350-4487(94)90086-8
- Roberts, H. H. (1997). Dynamic changes of the Holocene Mississippi river delta plain: the delta cycle. *J. Coast. Res.* 13 (3), 605–627. Available at: <https://www.jstor.org/stable/4298659>.
- Sallenger, A. H. (2000). Storm impact scale for barrier islands. *J. Coast. Res.* 16 (3), 890–895. Available at: <https://www.jstor.org/stable/4300099>.
- Spencer, T., Brooks, S. M., Evans, B. R., Tempest, J. A., and Möller, I. (2015). Southern north Sea storm surge event of 5 December 2013: water levels, waves and coastal impacts. *Earth-Sci. Rev.* 146, 120–145. doi: 10.1016/j.earscirev.2015.04.002
- Stanley, D. J., and Warne, A. G. (2000). Worldwide initiation of holocene marine deltas by deceleration of sea-level rise. *Science* 265 (5169), 228–231. doi: 10.1126/science.265.5169.228
- Stanley, D. J., and Chen, Z. (2000). Radiocarbon dates in china's Holocene Yangtze delta: record of sediment storage and reworking, not timing of deposition. *J. Coast. Res.* 16 (4), 1126–1132.
- Stanley, D. J., and Warne, A. G. (1994). Worldwide initiation of holocene marine deltas by deceleration of sea-level rise. *Science* 265 (5169), 228–231. doi: 10.1126/science.265.5169.228
- Stanley, D. J., and Warne, A. G. (1998). Nile Delta in its destruction phase. *J. Coast. Res.* 14 (3), 795–825. Available at: <https://www.jstor.org/stable/4298835>.
- Swindles, G. T., Galloway, J. M., Macumber, A. L., Croudace, I. W., Emery, A. R., Wouds, C., et al. (2018). Sedimentary records of coastal storm surges: Evidence of the 1953 north Sea event. *Mar. Geol.* 403, 262–270. doi: 10.1016/j.margeo.2018.06.013
- Syvitski, J. P., Kettner, A. J., Overeem, I., Hutton, E. W., Hannon, M. T., Brakenridge, G. B., et al. (2009). Sinking deltas due to human activities. *Nat. Geosci.* 2 (10), 681–686. doi: 10.1038/ngeo629
- Tan, Q. (1975). *The historical atlas of China (Vol. 7-8)* (Shanghai: Chinese Map Publishing House).
- Wang, X. (2010). The historical law study of Shandong coastal storm surge disaster-centered on the Ming and Qing dynasty, (1374-1911) [dissertation thesis]. (Qing Dao: Ocean University of China).
- Wang, H., Wu, X., Bi, N., Li, S., Yuan, P., Wang, A., et al. (2017). Impacts of the dam-orientated water-sediment regulation scheme on the lower reaches and delta of the yellow river (Huanghe): A review. *Global Planet. Change.* 157, 93–113. doi: 10.1016/j.gloplacha.2017.08.005
- Wang, H., Yang, Z., Saito, Y., Liu, J. P., Sun, X., and Wang, Y. (2007). Stepwise decreases of the huanghe (Yellow river) sediment load, (1950 – 2005): Impacts of climate change and human activities. *Global Planet. Change* 57, 331–354. doi: 10.1016/j.gloplacha.2007.01.003
- Wang, Q., Zhong, S., Li, X., Zhan, C., Wang, X., and Liu, P. (2016). Supratidal land use change and its morphodynamic effects along the eastern coast of laizhou bay during the recent 50 years. *J. Coast. Res.* 74, 83–94. doi: 10.2112/S174-008.1
- Wang, Q., Zhou, H., Cheng, K., Chi, H., Shen, C., Wang, C., et al. (2015). The climate reconstruction in Shandong peninsula, north China during the last millennia based on stalagmite laminae. *Clim. Past* 11, 4643–4668. doi: 10.5194/cpd-11-4643-2015
- Wu, X., Bi, N., Xu, J., Nittrouer, J. A., Yang, Z., Saito, Y., et al. (2017). Stepwise morphological evolution of the active yellow river (Huanghe) delta lobe, (1976–2013): Dominant roles of riverine discharge and sediment grain size. *Geomorphology* 292, 115–127. doi: 10.1016/j.geomorph.2017.04.042
- Xu, Q., Meng, L., Yuan, G., Teng, F., Xin, H., and Sun, X. (2020). Transgressive wave-and tide-dominated barrier-lagoon system and sea-level rise since 8.2 ka recorded in sediments in northern bohai bay, China. *Geomorphology* 352, 106978. doi: 10.1016/j.geomorph.2019.106978
- Xue, C. (1993). Historical changes in the Yellow River delta, China. *Mar. Geol.* 113 (3–4), 321–330. doi: 10.1016/0025-3227(93)90025-Q
- Yang, S., Fan, J., Shi, B., Bouma, T., Xu, K., Yang, H., et al. (2019). Remote impacts of typhoons on the hydrodynamics, sediment transport and bed stability of an intertidal wetland in the Yangtze delta. *J. Hydrol.* 575, 755–766. doi: 10.1016/j.jhydrol.2019.05.077
- Yang, Z., Ji, Y., Bi, S., Lei, K., and Wang, H. (2011). Sediment transport off the huanghe (Yellow river) delta and in the adjacent bohai Sea in winter and seasonal comparison. *Estuar. Coast. Shelf S.* 93 (3), 173–181. doi: 10.1016/j.ecss.2010.06.005
- Zeng, L., Zhan, C., Wang, Q., Liu, X., Wang, L., Li, X., et al. (2021). Sediment coarsening in tidal flats and stable coastline of the abandoned southern yellow river Sub-delta in response to fluvial sediment flux decrease during the past decades. *Front. Mar. Sci.* 8. doi: 10.3389/fmars.2021.761368
- Zhang, W., Xu, Y., Guo, L., Lam, N., Xu, K., Yang, S., et al. (2022). Comparing the Yangtze and Mississippi river deltas in the light of coupled natural-human dynamics: Lessons learned and implications for management. *Geomorphology* 399, 108075. doi: 10.1016/j.geomorph.2021.108075
- Zhan, C., Wang, Q., Cui, B., Zeng, L., Dong, C., Li, X., et al. (2020). The morphodynamic difference in the western and southern coasts of laizhou bay: Responses to the yellow river estuary evolution in the recent 60 years. *Global Planet. Change* 187 (3), 103138. doi: 10.1016/j.gloplacha.2020.103138
- Zhou, L., Liu, J., Saito, Y., Zhang, Z., Chu, H., and Hu, G. (2014). Coastal erosion as a major sediment supplier to continental shelves: example from the abandoned old huanghe (Yellow river) delta. *Cont. Shelf Res.* 82, 43–59. doi: 10.1016/j.csr.2014.03.015
- Zhuang, Z., Xu, W., and Li, X. (1991). The coastline evolution on the south coast of the bohai Sea since 6 ka B.P. *J. Ocean Univ. QingDao* 2, 99–110. doi: 10.16441/j.cnki.hdxh.1991.02.010